BUILDING AN AUTOMATED CRATER RECOGNITION ROUTINE. M. P. Mendenhall, *Dept. of Physics, Washington University in St Louis, St Louis, MO, USA, (m.praetorius@gmail.com)*, T. F. Stepinski, *Lunar and Planetary Institute, Houston TX 77058-1113, USA, (tom@lpi.usra.edu)*.

1 Introduction

The Mars Orbiter Laser Altimeter (MOLA) instrument on the Mars Global Surveyor orbiter has produced a large volume of topography data in which craters are prominently displayed. Figure 1 shows a small example of such a topography dataset. The current state-of-the-art in crater identification and characterization is a summer intern manually scrutinizing topography images. Such a labor-intensive approach is susceptible to being overwhelmed by the sheer volume of data returned by current and future missions. Automation of the crater cataloging process is a necessary to make full use of the extensive topography datasets available.

The *Cratermatic* topography analysis program **(1)** was developed to meet this need. *Cratermatic* performs a multi-step process to

- identify approximate crater centers

- determine the full extent of each crater candidate

- eliminate many false-positive identifications

- catalog basic characteristics of the identified craters

Application of *Cratermatic* to various sample datasets produces results which compare favorably with previous crater locating routines **(2)**, while providing a basis for more in-depth characterization of each crater.
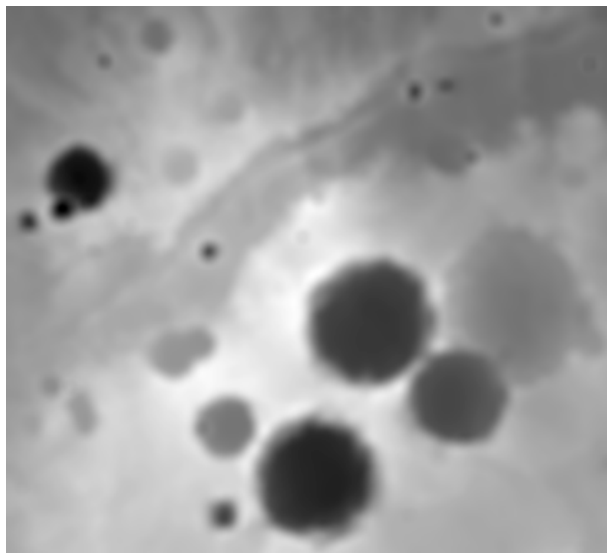
Figure 1: A small elevation dataset
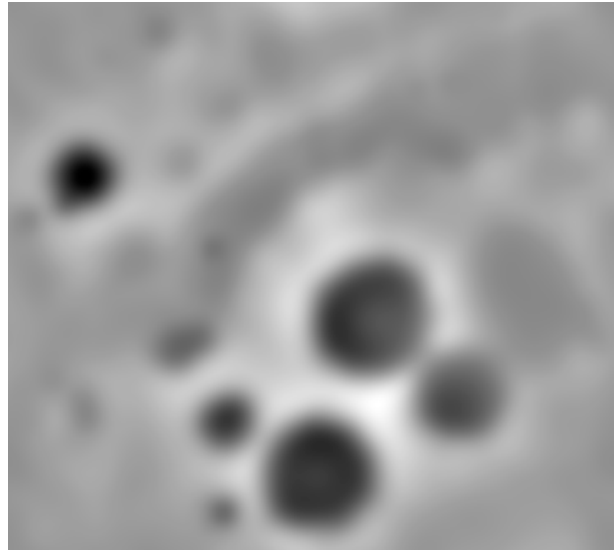
Figure 2: Radius 20 C-Transform of the Figure 1 dataset

2 Approximating crater locations

Craters come in all sizes, often with smaller craters nested inside larger craters. By first searching for smaller craters (typically about 5 pixels radius in the topography data) then proceeding to successively larger craters in subsequent steps, the *Cratermatic* routine avoids the difficulty of simultaneously identifying nested craters.

Suppose the topography landscape of a region $S \subset \mathbb{R}^2$ is described by the differentiable function $z : S \rightarrow \mathbb{R}$. On an ideal landscape, each local minima of z would be the center of one crater. For real data, however, most local minima are not craters and most craters contain several local minima.

For an ideal crater, the gradient $\vec{\nabla} z$ is strongest on the crater rim and points outward from the center. Thus, to find the center of craters with a radius of approximately r, we look for locations "pointed away from" by the gradient within a radius $\sim r$. This motivates the crater-finding transform (C-Transform)

$$C \circ z : \vec{\mathbf{x}} \mapsto \iint_S e^{-\frac{\left|\vec{\mathbf{x}} - \vec{\mathbf{x}}'\right|^2}{2r^2}} \vec{\nabla} z(\vec{\mathbf{x}}') \cdot \frac{\vec{\mathbf{x}}' - \vec{\mathbf{x}}}{\left|\vec{\mathbf{x}}' - \vec{\mathbf{x}}\right|} d\vec{\mathbf{x}}'$$

Craters with radii near r will produce local minima in the transformed surface $C \circ z$. The C-Transform behaves similarly to a Gaussian convolution, insofar as it smoothes out features smaller than the characteristic size r. The C-Transform also suppresses low-frequency components in the image, leveling out any slowly changing background gradients. As a result,
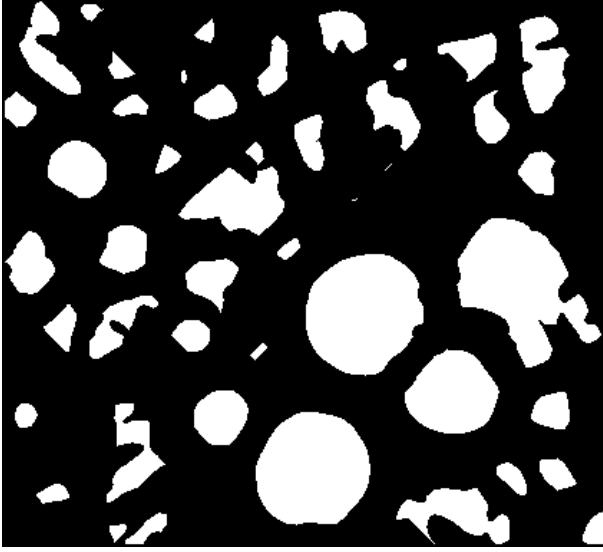
Figure 3: Upward-concave regions (white areas) of the radius 20 C-Transform (Figure 2)

Figure 4: Regions of Figure 3 expanded to cover whole crater

a crater of the appropriate size creates a smooth, pronounced basin in the transform surface. These basins provide a starting point for the *Cratermatic* search process. Figure 2 shows the 20 pixel radius C-Transform of the Figure 1 topography dataset.

3   Determining crater extents

Using the C-Transform as a guide for where to look, the actual extent of each crater must be determined. First, the C-Transform is used to approximate the area covered by the crater. The approximated area provides sufficient statistics about the character of the crater for the precise extent to be determined from the elevation data.

The approximate crater regions are determined from the upward-concave basins in the C-Transform. Concavity is determined by calculating the discrete second derivative along four lines through each point in the C-Transform image; those points with positive second derivatives in all four directions are considered to be upward-concave. Figure 3 shows the concavity determination applied to the radius 20 C-Transform of Figure 2.

In practice, these upward convex "crater core" regions tend to cover the actual crater region to about half-way up the crater walls. A core region thus contains enough of the crater to make a rough estimate of the crater wall's slope. Knowing approximately what to look for based on the topography contained in the core region, each core region is expanded outward to include the entire interior of the crater. Figure 4 shows the expanded regions based on the core regions of Figure 3.

4   Characterizing crater regions

The expanded regions from the preceding step are a mixture of actual craters and false-positive identifications. The tasks of characterizing the actual craters and eliminating the false-positive regions are carried on simultaneously.

One fundamental characteristic of a crater is the shape of the above determined area. To first order, this is a circle, but many craters are significantly elliptical. Let $U \subset \mathbb{R}^2$ denote the region covered by the crater. We may define the center of the crater by the "center of mass" of U, $\vec{c} = \frac{\iint_U \vec{x} d\vec{x}}{\iint_U d\vec{x}}$. Since the crater's shape is convex, or at least starlike about $\vec{c}$, we can describe the shape by its radius as a function of angle around $\vec{c}$, $r(\theta)$. Writing $r(\theta)$ as a Fourier series,

$$r(\theta) = r_0 \cdot \left(1 + \sum_{n=1}^{\infty} a_n \sin n\theta + b_n \cos n\theta\right)$$

$$\pi r_0^2 \equiv \iint_U d\vec{x}; \ a_n \equiv \frac{\iint_U \sin n\theta \, d\vec{x}}{\iint_U d\vec{x}}; \ b_n \equiv \frac{\iint_U \cos n\theta \, d\vec{x}}{\iint_U d\vec{x}}$$

The terms r_0, a_2, and b_2 provide a good second-order description of crater shape ($a_1 \approx b_1 \approx 0$ due to the choice of $\vec{c}$ for the center). Large values for the higher coefficients indicate a lumpy, irregular shape that can be eliminated from the list of crater candidates.

The same approach may be applied to the crater gradient by writing the average gradient $\vec{g}$ as a function of angle θ around the center point $\vec{c}$ in terms of a Fourier series,
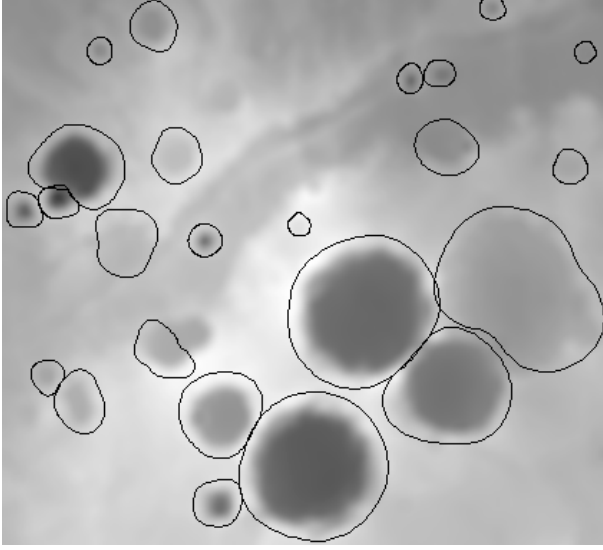
Figure 5: Identified craters from the Figure 1 dataset, with outlines generated from the first 6 terms in the series for $r(\theta)$

$$\vec{\mathbf{g}}(\theta) = \sum_{n=0}^{\infty} \left(a_n \sin n\theta + b_n \cos n\theta \right) \hat{\mathbf{x}}$$

$$+ \sum_{n=0}^{\infty} \left(c_n \sin n\theta + d_n \cos n\theta \right) \hat{\mathbf{y}}$$

$$a_n \equiv \frac{\iint_U \frac{\partial}{\partial x} z(\vec{\mathbf{x}}) \cdot \sin n\theta \, d\vec{\mathbf{x}}}{\iint_U d\vec{\mathbf{x}}}, \text{ etc.}$$

For an ideal crater, b_1 and c_1 are the dominant coefficients, while $b_0 \hat{\mathbf{x}} + d_0 \hat{\mathbf{y}}$ gives the average background slope for the crater region. Large magnitudes for other coefficients indicate non-crater regions.

False-positive regions are identified by un-craterlike coefficients in the $r(\theta)$ and $\vec{\mathbf{g}}(\theta)$ series, and are removed from the final list of craters. Figure 5 shows the final result of running *Cratermatic* on the Figure 1 dataset, which combines the craters found for C-Transforms with radii of 5, 10, 20, and 40 pixels.

5   Findings and future work

The present *Cratermatic* algorithm leaves much room for improvement. All but the most marginal craters seem to be represented at the C-Transform basin stage, but so are a vast number of false positive identifications. The current crater core expansion method is suitable for well-formed, isolated craters, but is not robust for craters with highly variable wall slopes or adjoining, external slope features. The choice of appropriate criteria for discerning false positives from craters needs more study and refinement. After removing the false positives, the crater regions should be further expanded to encompass any outward-sloping rim edge, to allow determination of the height of the crater rim above the surrounding ground level.

6   References

(1). M.P. Mendenhall, *http://cratermatic.sourceforge.net*, 2006.

(2). B.D. Bue and T.F. Stepinski, Machine Detection of Martian Impact Craters from Digital Topography Data, submitted to *IEEE Transactions on Geoscience and Remote Sensing*, 2006.